Research on Engineering Structures & Materials
journal homepage: http://jresm.org
MIM Research Group

Research Article

Fracture behaviors and optimizations of friction stir spot welded and friction stir clinched hybrid aluminum/acrylonitrile butadiene styrene joints

Michael Kanisuru Adeyeri[1,a], Olatunji Oladimeji Ojo[*1,b], Adefemi Oluseye Adelusi[2,c]

[1]*Department of Industrial and Production Engineering, Federal University of Technology Akure, Nigeria.*
[2]*Department of Mechanical Engineering, Federal University of Technology Akure, Nigeria*

Article Info

Article history:
Received 10 Aug 2021
Revised 20 Nov 2021
Accepted 30 Nov 2021

Keywords:

Friction stir spot welding;
Friction stir clinching;
Aluminum alloy;
Acrylonitrile butadiene styrene polymer;
Fracture;
Mechanical properties;
Microstructure

Abstract

This study compares and optimizes the friction stir clinched and friction stir spot welded hybrid aluminum/acrylonitrile butadiene styrene polymer (Al/ABS) joints. The mechanical and fracture behaviors of the respective hybrid joints were investigated. The results show that the friction stir spot welded Al/ABS joint exhibited a higher tensile-shear failure load. The presence of higher deformation (protrusion-aided) and deeper tool profile-induced hole (stress raiser) in the friction stir clinched Al/ABS joint impaired the loadbearing resistance of the joint. The optimum tensile-shear failure loads of the friction stir spot welded, and friction stir clinched Al/ABS joints are 932 and 509 N respectively. Three fracture modes, namely unbuttoning, circumferential-partial Al in-polymer shearing, and mid-nugget shearing modes, ensue in both joint categories. Protrusion-aided deformation is not desirable for the improved performance of the hybrid Al/ABS joint. Friction stir spot welding is thus recommended for the fabrication of hybrid metal/polymer.

1. Introduction

The use of hybrid aluminum and polymeric materials has gained tremendous acceptance in modern manufacturing industries such as aerospace, transportation, and drone technology due to their desirable properties [1]. Aluminum has low density, high strength, and high corrosion resistance [2] while polymers are lightweight materials having long chain macro-molecules (with covalent bond) and with low thermal stability, high specific strength, high elastic modulus, and good flexibility. However, the joining of Al and polymers is difficult to achieve due to the disparity in the physiochemical properties of the materials. The traditional joining techniques such as adhesive bonding, riveting, and screwing are not desirable for joining Al and polymers due to shortcomings such as weight addition, and easily impaired adhesive-bonded interface between Al and polymer in a wet environment [4] [5][6][7]. Porosity, formation of reaction layers, impact-induced damages, and poor strength are also challenges of joining Al and polymers via the use of fusion-based techniques such as laser or hybrid laser welding processes [8][9]. There is consequently a need to explore, modify, and optimize other novel joining alternatives such as friction stir-based processes to reduce weld defects and improve the performance of hybrid Al/polymer joints.

*Corresponding author: ojooladimeji90@yahoo.com
[a] orcid.org/0000-0001-6640-409X; [b] orcid.org/0000-0002-6581-1168; [c] orcid.org/0000-0002-9645-7050
DOI: http://dx.doi.org/10.17515/resm2021.329me0810

Friction stir-based welding processes have been identified as suitable techniques for joining dissimilar Al and polymer materials [10]. This approach leverages on the nonmolten plastic deformation, inter-material flow effects [11][12], mechanical interlocks, molecular adhesion, Al-C-O reaction or physiochemical bonding [13][14][15], and van der Waal's bonding for sound hybrid Al/polymer joints [16][17][18][19]. Recently, Ojo [20] investigated macro-/micro-mechanical interlocking improvement of the Al/ABS polymer joint via the use of pre-fabricated unthreaded- and threaded-hole friction stir spot welding processes. The variances of this new friction stir-based spot joining approach are friction stir spot welding (FSSW) and friction stir cinching (FSC), which require comparative elucidation and optimization. FSC is a modified or advanced method of mechanical clinching that reduces joining force (by 40-60 times) and cracks formation while improving material flow and metallurgical bonding in similar/dissimilar joints [19]. A paucity of information on FSC of metal/polymer joints exists in literature while a few reports are available on mechanical clinching of metal/polymer [21][22][23][24]. The impact of friction-assisted clinching or FSC process on the metal/polymer materials is yet to receive full clarification in literature. Recently, Lambiase and Paoletti [25] investigated the friction-assisted clinching of Al and carbon fiber-reinforced polymer. It was revealed that the utilization of friction clinching increased the joint's formability (material flow) as compared to the conventional clinched joint (having poor ductility). However, there is a need to improve the performance of metal/polymer joints via effective optimization techniques such as single/multi-objective Taguchi-based approaches [26-28], NSGA-II algorithm [29], and model-based optimization method [30].

Based on the paucity of information on the friction stir clinched metal/polymer hybrid joints and the need to identify the suitable joining approach, this research compares and optimizes the friction stir clinching and friction stir spot welding of aluminum and polymer materials. For the first time, the clarification, comparison, and optimization of mechanical interlocking-induced friction stir-based spot joining approaches (friction stir clinching and friction stir spot welding) of aluminum alloy and acrylonitrile butadiene styrene (ABS) polymer were provided in an attempt to further explore the performance-desirability and weldability of hybrid metal/polymer joints. The mechanical, microstructure, and fracture behaviors of the respective joints are studied while the joining processes were optimized.

2. Materials and Method

The materials used in this research are aluminum alloy and acrylonitrile butadiene styrene (ABS) polymer sheets with thicknesses of 3.0 and 4.0 mm respectively. The chemical composition of the Al alloy is shown in Table 1. The base materials (sheets) were cleaned and cut into the dimensions of 100 mm by 30 mm. The sheets were placed in an overlapped configuration with the Al sheet placed as the top sheet. Friction stir spot welding (FSSW) and friction stir clinching (FSC) processes were employed to join the overlapped sheets as illustrated in Fig. 1. A pre-drilled hole was created in the die before the FSC process. The hole diameter and depth in the die are 7.0 mm and 4.0 mm respectively as illustrated in Fig. 1. The FSC and FSSW processes were carried out on an MV-2 Maximill milling machine with welding tools having the same morphology. The welding tool (for both FSSW and FSC processes) was fabricated from high-speed steel (HSS). Conical shoulder cylindrical pin tools having 12 mm shoulder diameter and 6 mm pin diameter were utilized for the joining processes, however, the pin length was 5.0 mm for the FSC process while it was 4.0 mm for the FSSW process. Some parameters were selected as ideal for this research based on previous research works in this field. Table 2 shows the parameter variation used for this study. The experiment was planned via the use of the Taguchi method while the L9 orthogonal array was employed for the welding processes. Table 3 shows the L9 orthogonal array for this study and the coding employed for each of the welding processes.

Table 1. Chemical Composition of Al Alloy

Elements	Mg	Mn	Zn	Ni	Sn	Sb	Cr	Al
Wt.%	5.0303	0.0393	0.1139	0.0529	0.0221	0.0485	0.0081	94.6748

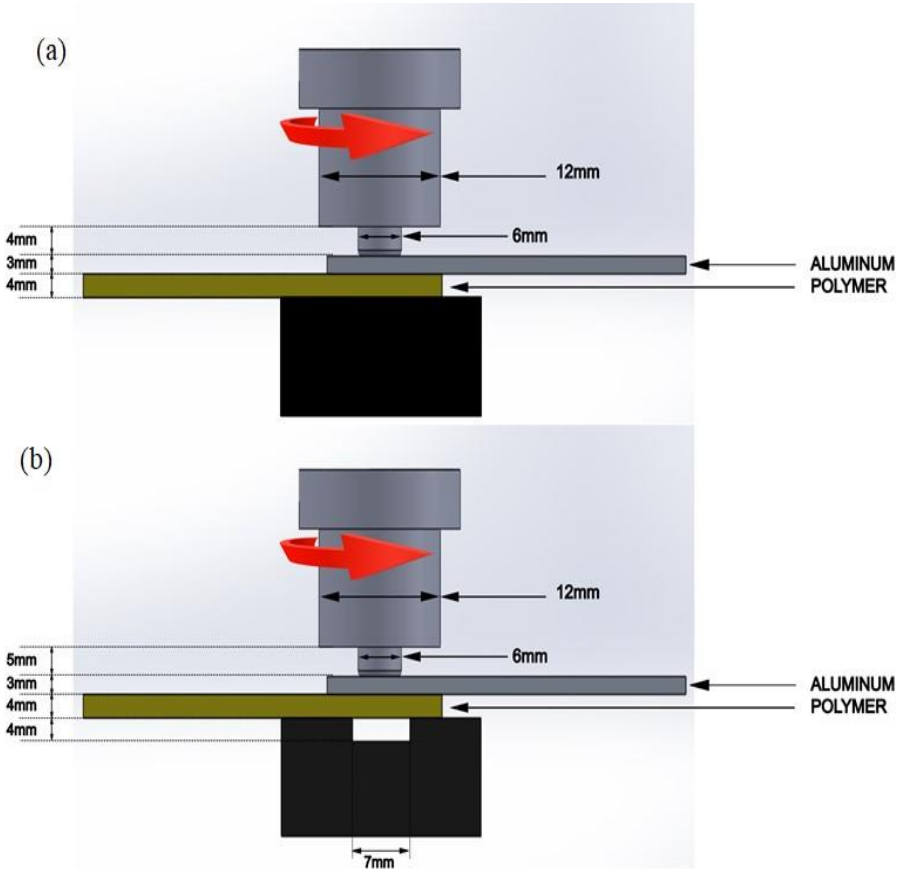

Fig. 1 Illustrations of the Friction Stir-Based Welding Processes (a) FSSW, (b) FSC

Table 2. FSSW and FSC Parameter Variation

S/N	Parameter	Unit	Variation
1	Tool rotational speed (A)	rev/min	900, 1120, 1400
2	Plunge depth (B)	Mm	5.5, 6.0, 6.5
3	Dwell time (C)	S	3, 4, 5

The temperatures at which the joining of the materials took place were recorded. The top Al plates were grooved to create slots for the placement of three K-type thermocouples A, B and C. Thermocouple C (T_C) was at 15 mm distance from the center of the joint, thermocouple B (T_B) was 6 mm away from C, and thermocouple A (T_A) was 6 mm away from B respectively as illustrated in Fig. 2. Fig. 3 shows the actual setup of the K-type thermocouples before the welding process. The temperature readings at three rotational

speeds (900 rpm, 1120 rpm, 1400 rpm) were taken with the use of a data logger in milliseconds.

Table 3. FSSW and FSC Experimental Run

Exp. No.	Tool rotational speed (rpm)	Plunge depth (mm)	Dwell time (s)	Code for FSC	Code for FSSW
1	900	5.5	3	A1	B1
2	900	6.0	4	A2	B2
3	900	6.5	5	A3	B3
4	1120	5.5	4	A4	B4
5	1120	6.0	5	A5	B5
6	1120	6.5	3	A6	B6
7	1400	5.5	5	A7	B7
8	1400	6.0	3	A8	B8
9	1400	6.5	4	A9	B9

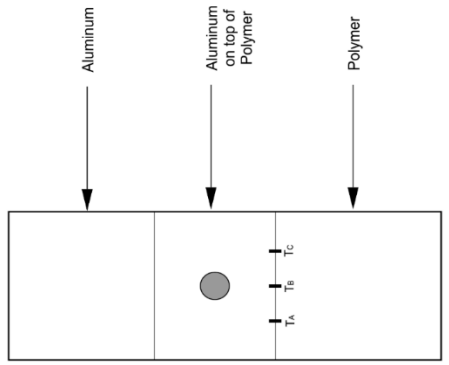

Fig. 2 Schematic Illustrations of K-Type Thermocouples

Fig. 3 Actual Setup Showing the Positioned Thermocouples

The microstructure of the as-welded samples was obtained by following the standard metallographic procedure. The as-welded FSSW and FSC joints were mounted on a Universal Testing Machine (Instron series 3369) to determine the tensile-shear failure

load of the irrespective joints under ASTM D3039 standard and at a strain rate of 5 mm/min. The average of three samples was taken as the actual tensile-shear failure load in this paper. The failed samples (during the tensile loading process) were examined under an optical microscope and in JOEL-JSM 7600F scanning electron microscope (SEM) to clarify the fracture of the joints. The Taguchi optimization approach was employed for the process parameter optimization of the two welding processes (FSSW and FSC) by using the MINITAB® 17 software to compute and plot the main effect plots for means and signal-to-noise (SN) ratio. The tensile-shear failure load was set as the output response for the process parameter optimization and the goal was to maximize this output response. The large-the better quality-characteristic or signal-to-noise ratio (SN ratio) expressed in Equation 1 was employed to reveal the effect of process/control factors on the tensile-shear failure load (response) of the joints. Where Y_i is the ith value of the tensile-shear failure load/response and n is the number of trials. The optimal (control) levels of the FSSW and FSC processes were derived from the effect plot as the levels with the maximum/highest SN ratio. The performance values of the optimal levels (for FSSW and FSC joints) are predicted via the use of Equations 2 and 3 [31] or Equation 4.

$$SN = -10\log_{10}\left[\frac{1}{n}\sum_{i=1}^{n}\frac{1}{Y_i^2}\right] \tag{1}$$

$$(SN)_{prediction} = (SN)_{mean} + \sum_{i=1}^{k}\left[\left(\widetilde{SN}\right)_i - (SN)_{mean}\right] \tag{2}$$

$$Y_{(prediction)} = \sqrt{\frac{1}{10^{\left(\frac{(SN)_{prediction}}{-10}\right)}}} \tag{3}$$

$$Y_{prediction} = Y_{mean} + \sum_{i=1}^{k}[Y_i - Y_{mean}] \tag{4}$$

Where $(SN)_{prediction}$ is the predicted signal-to-noise ratio (performance characteristic in dB) at optimal conditions/levels, $(SN)_{mean}$ is the mean of all SN ratios, $\left(\widetilde{SN}\right)_i$ is the highest S/N ratios that provide the optimal level, k is the number of effective process parameters (factors) that significantly influence the optimal conditions, $Y_{(prediction)}$ is the predicted tensile-shear failure of the Al/ABS joint, and Y_{mean} is the average of the performance characteristic in each of the welding processes.

3. Results and Discussion

3.1 Surface Appearance and Al/ABS Bonding

The surface appearances of the as-welded hybrid Al/ABS joints are shown in Fig. 4. Fig. 4a and b reveal the top views of the FSSW and FSC-welded hybrid Al/ABS joints respectively. The tool-induced inherent profiles facilitated by the tool plunging effect are present on the top views of the respective joints. The presence of plasticized Al alloy around the tool-induced cavity is also palpable in Fig. 4a and b. This attribute is associated with the frictional heat input-aided material flow effect. According to Ojo et al. [32], the intense frictional heat generated at the tool shoulder surface together with the tool plunging effect is responsible for the formation of surface-flash/plasticized material. The tool pin has been reported to facilitate material shearing and upward extruding material flow while the tool shoulder aids a combined compressive and shearing effect on the Al side of the hybrid joint

[33]. This phenomenon leads to the observed circumferential expelled flash around the tool-induced weld nugget in Fig. 4a and b. On the other hand, the reverse sides or back views of the hybrid Al/polymer joints are shown in Fig. 4c and d. Bulk protrusion due to the pre-drilled hole in the die is conspicuous in the FSC joint (see Fig. 4c) while a flat surface (no protrusion) with discernable evidence of embedded plasticized Al alloy is revealed in Fig. 4d. The protrusion in the FSC joint allows for interlocking (protrusion-aided interlocking) of the aluminum and the polymer as both the polymer and Al flow into the die during the combined tool plunging and rotating actions. This occurrence implies that inherent nugget-interlocking is established in the FSSW joint whereas a combination of somewhat nugget-interlocking and protrusion-aided interlocking is formed in the FSC joint. More material plasticization is thus adjudged to be experienced in the FSC welded hybrid Al/ABS owing to the surface bulk protrusion at the back view of the joint.

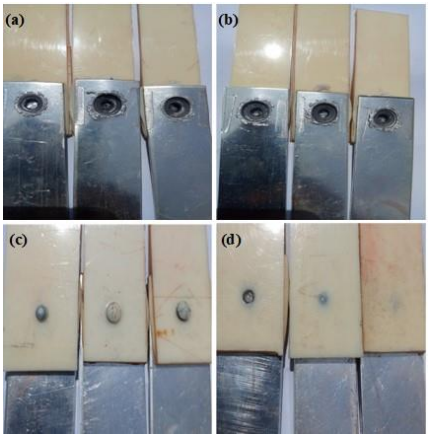

Fig. 4 Surface Appearances of Hybrid Al/ABS Joints, (a) Front Views of FSSW Joint, (b) Front Views of FSC Joint, (c) Back Views of FSC Joint, (d) Back Views of FSSW Joint

The bonding mechanisms in the FSC and FSSW welded Al/ABS joints are similar and two forms of bonding mechanism are observed in the hybrid Al/ABS joints in Fig. 5. The interlocked/shear-induced bonding ensues at the stir zone (see Fig. 5a) while adhesion bonding occurs at the Al/ABS interfacial region (see Fig. 5b) of the hybrid Al/ABS joints. The rotating tool induces a shearing effect on the Al alloy (during the welding processes) to form embedded (sheared) Al alloy within the re-solidified ABS polymer (at the stir zone) as observed in Fig. 5a. This phenomenon creates mechanical interlocking between the Al alloy and the ABS polymer. The frictionally induced melting of the polymer creates good wettability at the interfacial region between the Al alloy and the ABS polymer. This phenomenon establishes adhesion bonding in the hybrid Al/ABS joint. Paidar et al. [17] stated that the melting of the polymer aids the wetting of the aluminum plate and therefore supports the adhesive bonding of the Al/polymer at the interfacial region close to the stir zone. Interfacial adhesive bonding and mechanical interlocking mechanisms are thus the salient factors responsible for the strength/performance of the hybrid Al/ABS joints.

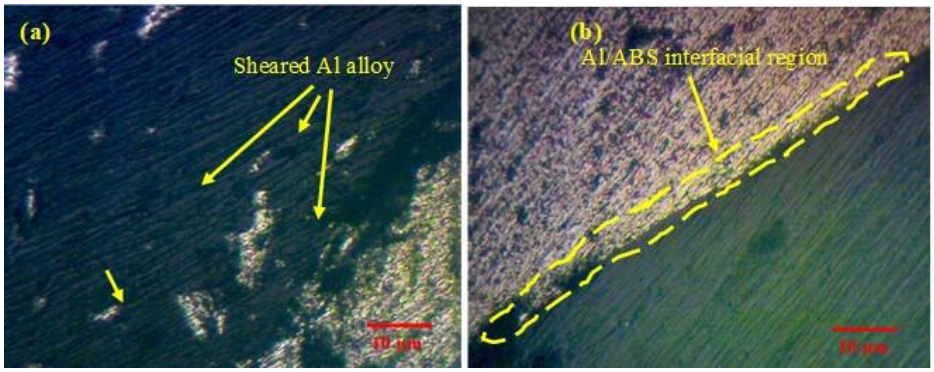

Fig. 5 Bonding Mechanisms in Hybrid Al/ABS Joints (a) Interlocked/Shear-Induced Bonding, (b) Adhesion Bonding

3.2 Temperature History

Fig. 6 shows the graphical representation of the in-situ temperature history of the welding process as the tool rotational speed is varied. The atmospheric temperature of 29.54°C was constant throughout the welding process as the local work done does not affect the atmospheric temperature. However, the relative humidity drops from 75.57% to 70.74% as the tool rotational speed is increased. This is because the air around the joint becomes warmer as the temperature increases. The temperature at which joining was carried out is revealed to increase with an increase in the tool rotational speed. Peak temperatures of 271, 332, and 370°C are attained at tool rotational speeds of 900, 1120, and 1400 rpm respectively during the joining process. An increase in tool rotational speed induces more stirring action on the weld nugget and this phenomenon consequently leads to a rise in the frictional and plastic deformational-induced heat input and it eventually leads to a rise in the peak temperature. The obtained temperatures (at 900, 1120, and 1400 rpm) are less than the melting point of pure aluminum alloy (660°C) but are higher than that of the polymer (160°C). This occurrence indicates that the Al alloy does not melt but deforms plastically during the joining process while the polymer melts and interlocks with the plasticized aluminum alloy after cooling/solidification. This corroborates the studies of Paidar et al. [17] as an increase in rotational speed increases the peak temperature, material flowability, and width of the heated zone and the stir zone around the tool probe. The temperature declines from peak temperature upon retraction of the rotating tool from the stir zone.

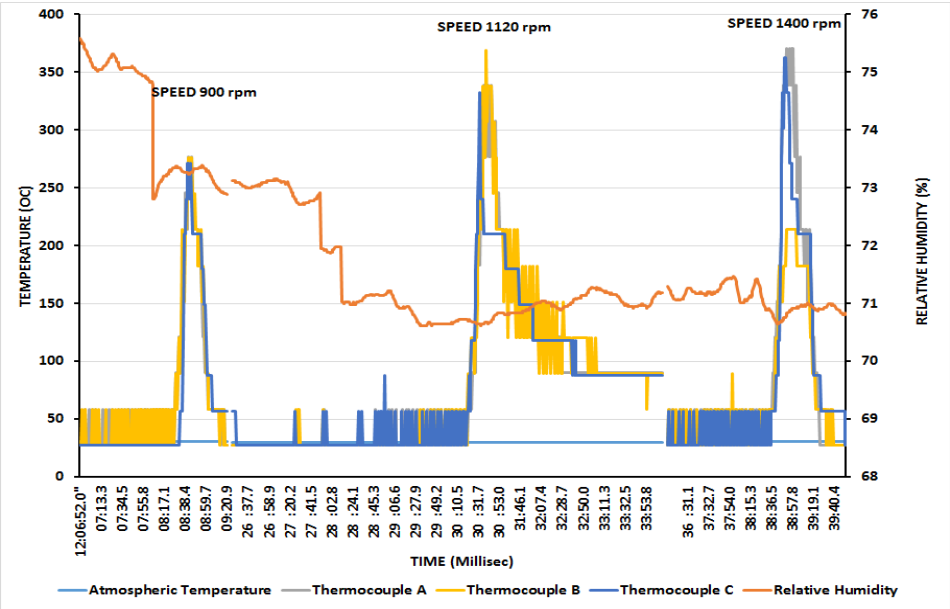

Fig. 6 Time -Temperature Series Graph of the Joining Process (900 rpm, 1120 rpm, 1400 rpm)

3.3 The Tensile Failure Load and Optimization

Table 4 shows the tensile results (average failure loads) and the signal-to-noise ratios (SN) of the hybrid FSC and FSSW joints respectively. The SN ratio is determined according to the performance characteristic of the higher-the better in Equation 1. The comparison of the failure loads of the hybrid FSC and FSSW joints under the same parameter combinations is shown in Fig. 7. It is observed that the failure loads of the FSSW joint are higher than those of the FSC joints. Although mechanical interlocking is formed in the FSC joint through the surface protrusion (exterior material flow), a lesser failure load is achieved with the FSC process. This phenomenon is attributed to more plasticization and deeper tool profile-induced hole effects in the FSC welded hybrid Al/ABS joint. It is adjudged that the intense plasticization (of the FSC joint) restrains the ability of the interlocked (protrusion) region of the hybrid Al/ABS joint to further ductility/formability while the deeper probe hole in the joint also limits the load-bearing ability of the joint as compared to the FSSW joint. Meanwhile, the presence of lesser probe-hole and nugget (interior) weld-material interlocking in the FSSW joint is considered to have favored load-bearing ability. This attribute is responsible for the better failure load or resistance in the FSSW joint when compared to the FSC joints. The maximum failure load of about 854 N (B2) and 449 N (A5) were obtained in the hybrid FSSW and FSC joints respectively at different parameter combinations. This observation shows that the process parameters have different degrees of influence on the FSSW and FSC processes.

Table 4. Tensile Results of FSSW and FSC Joints

Exp. No	Average failure load - FSC (N)	SN Ratio- FSC (dB)	Average failure load - FSSW (N)	SN Ratio – FSSW (dB)
1	134.7535	42.5908	765.1398	57.6748
2	403.5896	52.1188	854.4721	58.6340
3	274.1934	48.7611	769.7438	57.7269
4	393.8353	51.9063	424.8038	52.5638
5	448.9113	53.0432	412.4872	52.3082
6	302.3972	49.6116	296.3023	49.4347
7	289.5255	49.2337	452.5064	53.1125
8	366.7095	51.2864	642.0259	56.1511
9	159.2026	44.0390	191.6125	45.6485

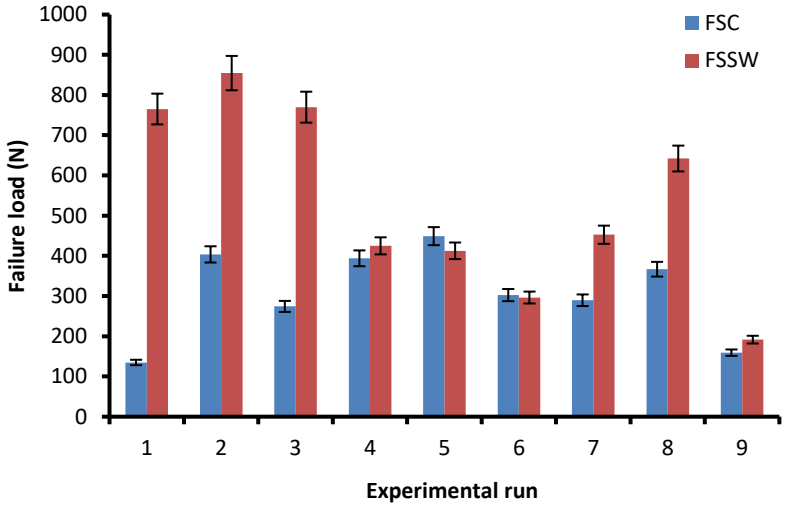

Fig. 7 Comparative Failure Loads of FSC and FSSW

The influences of the process parameters on the failure load of the FSSW and FSC joints are thus examined via the use of response tables (see Tables 5 and 6). The results rank the plunge depth as the most dominant welding parameter in the FSC process, follow by the tool rotational speed and the dwell time respectively. On the other hand, tool rotational speed is the most significant in the FSSW joint, follow by plunge depth and dwell time respectively. Table 7 and Table 8 corroborate the influences of the process parameters on the tensile-shear failure loads of the FSC and FSSW joints respectively via the analysis of variances (ANOVA) based on a 95% confidence level. The contributions of the tool rotational speed, plunge depth, and dwell time on the tensile-shear failure loads of the FSC joints are 26.07, 47.71, and 8.33% respectively (see Table 7). On the other hand, tool rotational speed and plunge depth had contributions of 72.73 and 16.61% on the tensile-shear failure loads of the FSSW joints respectively. Plunge depth significantly affects the formability of the ABS polymer and plays a significant role in achieving Al/ABS interlocks

(surface/exterior) in the FSC joints. This finding agrees with the works of Mubiayi et al. [34] as an increase in plunge depth leads to an increase in failure load.

Table 5. Response Table for Signal to Noise Ratios (FSC)

Level	Tool rotational speed (A)	Plunge depth (B)	Dwell time (C)
1	47.82	47.91	47.83
2	51.52	52.15	49.35
3	48.19	47.47	50.35
Delta	3.70	4.68	2.52
Rank	2nd	1st	3rd

Table 6. Response Table for Signal to Noise Ratios (FSSW)

Level	Tool rotational speed (A)	Plunge depth (B)	Dwell time (C)
1	58.01	54.45	54.42
2	51.44	55.70	52.28
3	51.64	50.94	54.38
Delta	6.58	4.76	2.14
Rank	1st	2nd	3rd

Table 7. Analysis of Variance (FSC)

Source	DF	Seq SS	Adj SS	Adj MS	F-Value	P-Value	Contribution
Rotational speed	2	24371	24371	12186	1.46	0.407	26.07%
Plunge depth	2	44594	44594	22297	2.67	0.273	47.71%
Dwell time	2	7784	7784	3892	0.47	0.682	8.33%
Error	2	16729	16729	8364			
Total	8	93478					

S: 91.4563; R-sq: 82.10%

Table 8. Analysis of Variance (FSSW)

Source	DF	Seq SS	Adj SS	Adj MS	F-Value	P-Value	Contribution
Rotational speed	2	313032	313032	156516	8.60	0.104	72.73%
Plunge depth	2	71481	71481	35741	1.96	0.337	16.61%
Dwell time	2	9518	9518	4759	0.26	0.793	2.21%
Error	2	36400	36400	18200			
Total	8	430431					

S: 134.908; R-sq: 91.54%

Based on the Taguchi method, the optimal parameter settings are the highest values of the SN ratios per process parameter (for the welding processes). Figs. 8 and 9 show the main effects plot for SN ratios of the FSC and FSSW joints respectively. The highest values of the SN ratios (from the main effects plot) are the peak points having red coloration in Figs. 8 and 9. The optimal parameter combinations for the FSC and FSSW processes are A2B2C3 (1120 rpm/6.0 mm/5 s) and A1B2C1 (900 rpm/6.0 mm/3 s) respectively. The optimized tensile-shear failure loads of the FSC and FSSW joints are 509 and 932 N respectively. The predicted values at the optimized settings could be adjudged to be close to the experimental values due to a lesser than 10% difference between these values. The

interrelationships between the response (tensile-shear failure load) and the independent process parameters are also revealed in the effects plot (see Figs. 8 and 9). An increase in tool rotational speed beyond level 2 (1120 rpm) causes a decline in the tensile-shear failure load of the FSC joint (see Fig. 8) while an increase in the tool rotational speed beyond level 1 (900 rpm) causes a decline in the tensile-shear failure load of the FSSW joint (see Fig. 9). The impacts of plunge depth and dwell time on the performances of both weld categories (FSC and FSSW joints) are similar. A rise in plunge depth (up to 6.0 mm) increases the tensile-shear failure load of both joints. Dwell time has a somewhat linear correlation with the tensile-shear failure of the FSC joint (see Fig. 8).

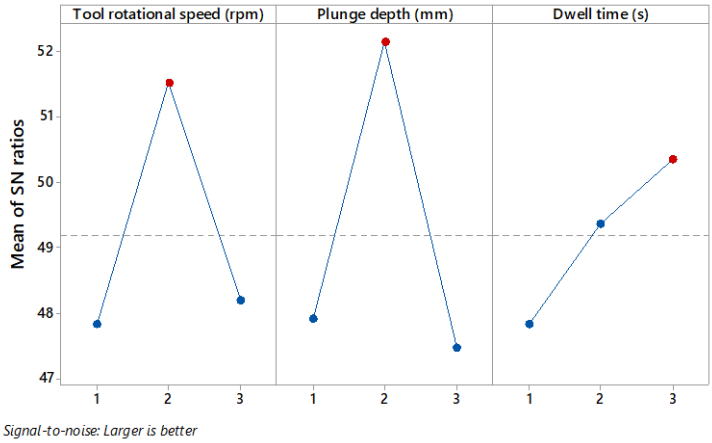

Fig. 8 Mean Effects Plot of SN Ratios for the FSC Joints

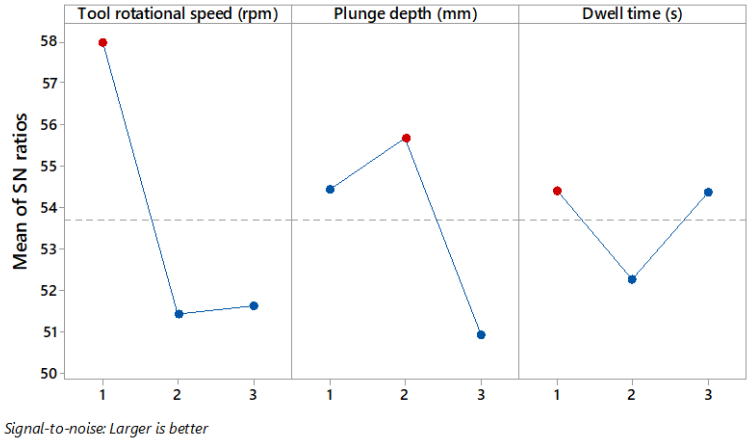

Fig. 9 Mean Effects Plot of SN Ratios for the FSSW Joints

3.4 Fractography

All the fracture patterns of the FSC and FSSW joints are examined (after tensile processing) and the unalike fracture patterns are selected for further assessment. The different interfacial fracture surfaces of the FSC and FSSW joints are provided in Tables 8 and 9 while their equivalent cross-sectional views (fracture paths) are shown in Fig. 10 respectively. The assessment of these images (Fig. 10 and Tables 8 and 9) indicates that

the FSSW and FSC joints exhibit somewhat close fracture modes. The fracture modes of the FSSW and FSC joints are thus carefully grouped into three based on the fracture paths (see Fig. 10) and the fracture outlook of the Al-ABS interfacial zones (see Tables 8 and 9). They are unbuttoning, circumferential-partial Al in-polymer shearing, and mid-nugget shearing modes respectively.

The unbuttoning fracture mode (UFM) is characterized by the ejection of the plasticized Al bulge from the inherent tool-induced polymer hole; a remnant of Al alloy is not left on the ABS polymer after fracture/sheet separation (in the FSSW and FSC joints). Complete delamination/retraction of the plasticized and interlocked Al alloy from the ABS polymer ensues in the hybrid Al/ABS joint (see the fracture coded "UFM" in Tables 8 and 9) due to the presence of no significant undercut and Al attachment at the interfacial ABS polymer side. The smooth surface appearance between the Al alloy and the ABS polymer indicates that there is no significant shear in the FSC and FSSW joints. Fig. 10a and b represent the observed UFM in the FSC and FSSW joints respectively. The red arrows indicate the fracture paths in the joints. Despite the presence of mechanical-induced macro-interlocking in the FSC and FSSW joints, delaminated fracture or unbuttoning fracture mode ensues in the Al/ABS joint. However, the sheared region in Fig. 10b is owing to the cutting/grinding or post fracture-induced shearing of the thin Al vortex region. The hybrid Al/ABS joints fabricated with the least plunge depth (5.5 mm) and high rotational speed (1400 rpm) exhibit the UFM in both the FSC and FSSW joints. This phenomenon is attributed to the dominant effect of heat-induced adhesion bonding and less amount of micro-interlocking required for fracture resistance (at the vortex and pin peripheral regions of the joints). The FSSW and FSC joints with the UFM mode had low tensile-shear failure loads. This occurrence implies that the pullout of the interlocked Al alloy from the ABS polymer sheet is easily achieved under tensile loading conditions.

The second fracture mode is the circumferential-partial Al in-polymer shearing mode (CPISM) shown in Tables 8 and 9 (see the samples coded "CPISM"), and Fig.1 0c and d. The CPISM has a little portion of the plasticized Al alloy embedded in the ABS polymer sheet upon sheet separation (see Tables 8 and 9). The red arrows indicate the fracture path in the FSC and FSSW joints. The complete pullout of the plasticized Al (interlocked) region is cutback during the tensile loading process in Fig. 10c and d. Also, the FSSW joint (see Fig. 10d) had fractures around the plasticized vortex edges (see the red circles) and fracture through the Al-ABS interfacial region. The fracture resistance causes crack initiation and tearing of the plasticized Al region due to phenomena such as suitable micro-mechanical interlocking at the pin peripheral region of the joint. This type of fracture mode is associated with an increase in the plunge depth beyond 5.5 mm. The CPISM mode is attributed to the thinning effect of the Al alloy at the vortex region within the weld nugget as the plunge depth is increased while the tool rotational speed is decreased to 1120 rpm. This corroborates the works of Lambiase et al. [35] as an excessive thinning of the Al neck was reported to facilitate this kind of fracture mode. A higher tensile-shear failure load is obtained in the joints that failed via the CPISM as compared to that of UFM.

Fig. 10e and f show the third fracture mode of the hybrid Al/ABS polymer joint termed as mid-nugget shearing mode (MSM). A mass of the plasticized Al alloy is left on the ABS polymer side and a tearing or shear-induced hole is left behind on the Al side. The volume of the plasticized and sheared Al alloy left on the ABS polymer side (after fracture) is larger than that of the CPISM. The cross-section of the hybrid Al/ABS joint (FSC) reveals complex shearing patterns around the mid-nugget region of the FSC joint (see Fig. 10e) while mid-nugget circumferential shearing ensues in the FSSW joint (see the red dotted/enclosed region in Fig. 10f). This category of fracture is achieved in the hybrid Al/ABS joints fabricated with a decrease in both the tool rotational speed (at 900 rpm) and plunge depth. The MSM fracture mode produces the highest fracture resistance or tensile-shear failure

loads in the FSSW and FSC joints. The synergy of decreased tool rotational speed and plunge depth is adjudged to have promoted sufficient micro-mechanical interlocking around the pin-induced peripheral region within the stir nugget (pin part of the tool facilitates shearing effect). The micro-mechanical interlocking of the Al alloy with the ABS polymer impedes the total pullout of the plasticized Al alloy from the ABS polymer during the tensile loading process. This attribute could be responsible for the MNSM fracture mode and a significantly high tensile-shear failure load of the hybrid Al/ABS joints (FSSW and FSC joints).

Table 8. Failed FSC Joints

FSC	Fracture	Aluminum Top (AT) view	Aluminum Base (AB) view	Polymer Top (PT) view	Polymer Base (PB) view
A2	CPISM				
	UFM				
A5	MSM				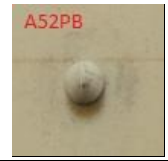

Table 9. Failed FSSW Joints

FSSW	Fracture	Aluminum Top (AT) view	Aluminum Base (PB) view	Polymer Top (PT) view	Polymer Base (PB) view
B1	CPISM				
B4	MSM		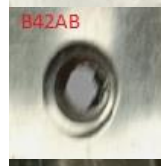		
B7	UFM				

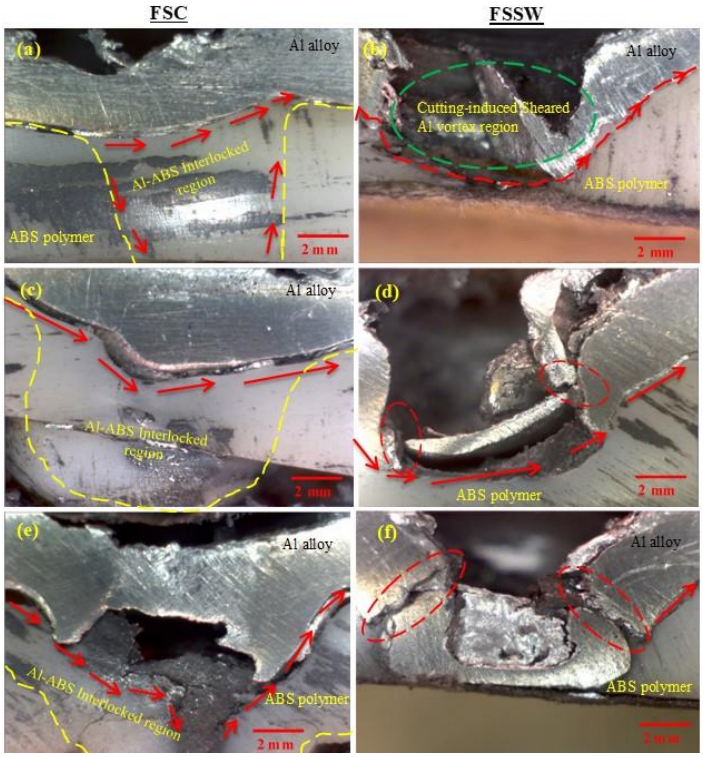

Fig. 10 Fracture Path of the FSC and FSSW Joints (a) Unbuttoning Fracture Mode in FSC, (b) Unbuttoning Fracture Mode in FSSW, (c) Circumferential-Partial Al in-Polymer Shearing Mode in FSC, (d) Circumferential-Partial Al in-Polymer Shearing Mode in FSSW Joint, (e) Mid-Nugget Shearing Mode in FSC, (f) Mid-Nugget Shearing Mode in FSS Joint

The fracture surfaces (ABS polymer sides) of the hybrid Al/ABS joints (FSC and FSSW) are further examined in a scanning electron microscope (SEM) as shown in Fig. 11. Fig. 11a and b reveal the presence of micro-pores of varying sizes (see the red and yellow arrows) in the FSC and FSSW samples with unbuttoning fracture mode (UFM) during high heat input/tool rotational speed (1400 rpm). The occurrence of pore coalescence and high porosity level in the joints (ABS polymer) is adjudged to have restrained the effect of micro-mechanical interlocking while favoring delaminated fracture between the Al alloy and the ABS polymer in the joints. The high area fracture of micro-pores in the FSC joints justifies the poor tensile-shear failure load in the FSC joints with UFM mode when compared to the FSSW joints. Similarly, Fig. 11c reveals the circumferential-partial Al in-polymer shearing mode (CPISM) of the FSC joint. Evidence of micro-pores and brittle fracture outlook with a significantly lesser porosity level is shown in Fig. 11c as compared to Fig. 11a. The lesser micro-pores in the FSC joint (Fig. 11c) are the major reason for the improvement in the tensile-shear failure load of the FSC joint over the samples that failed via UFM. Fig. 11d shows the evidence of polymer tearing morphology in the FSSW joint that failed through CPSIM. This occurrence implies that the ABS polymer exhibits ductile fracture mode during the tensile loading process when compared to the brittle fracture observed in Fig. 11c. Favorable fracture mode (see Fig. 11e and f) is revealed in the joints fabricated at low tool rotational speed (900 rpm). Fig. 11e and f reveal the mid-nugget shearing mode (MSM) of the FSC and FSSW joints respectively. The fracture of the ABS

polymer is observed in Fig. 11e. Ductile fracture is observed in the FSSW joint (having MSM mode in Fig. 11f) due to the presence of dimples on the fracture surface of the joint. Such ductile fracture has been attributed to the necking effect before the final failure. The observed occurrence reveals that the plasticized and interlocked Al attachment to the ABS polymer side undergoes some level of ductility before the final failure of the Al/ABS joint (FSSW). The practical fracture morphologies of the FSC and FSSW joints justify the reason for higher tensile-shear failure loads in FSSW joints as compared to the FSC joints.

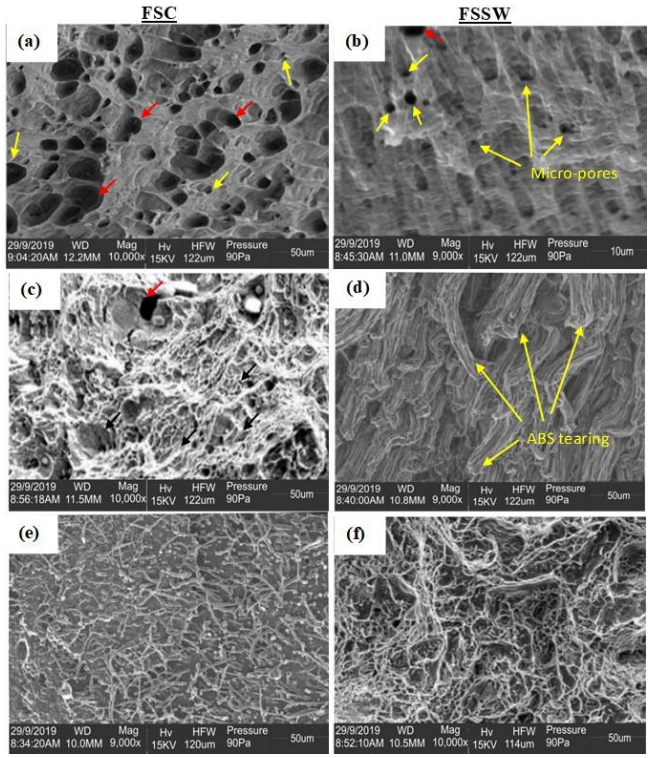

Fig. 11. SEM Images of the Fracture Surface (a) Unbuttoning Fracture Mode in FSC, (b) Unbuttoning Fracture Mode in FSSW, (c) Circumferential-Partial Al in-Polymer Shearing Mode in FSC, (d) Circumferential-Partial Al in-Polymer Shearing Mode in FSSW Joint, (e) Mid-Nugget Shearing Mode in FSC, (f) Mid-Nugget Shearing Mode in FSS Joint

4. Conclusion

The friction stir clinching and friction stir spot welding processes of aluminum alloy and acrylonitrile butadiene styrene sheets were successfully carried out. The optimization, mechanical, and fracture behaviors of the fabricated hybrid joints were investigated and compared. The findings of this study are summarized as follow:

- The synergy of interlocked/shear-induced bonding (micro-mechanical interlocking) at the stir zone and adhesion bonding at the Al/ABS interfacial region constitutes the noticeable bonding mechanisms of the hybrid Al/ABS joints. However, the interlocked/shear-induced bonding had the dominant loadbearing resistance on the Al/ABS joints due to the presence of sheared ABS

polymer at the stir zone as compared to the observed sheet separation/delamination at the Al/ABS interface after tensile tests.

- The tensile-shear failure load of the friction stir spot welded Al/ABS joints is higher than the friction stir clinched counterparts due to a higher plunging-induced deformation and deeper tool profile-induced hole (stress raiser) in the friction stir clinched joint. Thus, the application of friction stir spot welding process is recommended for the dissimilar welding of Al and ABS polymer materials.
- Plunge depth has the dominant impact on the tensile-shear failure load of the friction stir clinched Al/ABS joint (having a contribution of about 48%) while tool rotational speed has the foremost influence on the failure load of the friction stir spot welded Al/ABS joint (having a contribution of about 73%).
- The optimized tensile-shear failure loads of the friction stir clinched and friction stir spot welded Al/ABS joints are 509 and 932 N respectively.
- The fracture modes of the hybrid Al/ABS joints include unbuttoning, circumferential-partial Al in-polymer shearing, and mid-nugget shearing modes. A high porosity level lessens the impact of micro-mechanical interlocking and aids both pore coalescence and Al-polymer delamination (unbuttoning mode) at 1400 rpm (high tool rotational speed) while the occurrence of micro-mechanical interlocking has a significant influence on the other fracture modes.

References

[1] Celalettin Y, Fatih K, Nurettin Y, Oguz D. A review on advanced joining techniques of multimaterial part manufacturing for automotive industry. International Journal of Material and Production Engineering, 2015; 5: 63-68.

[2] Zhang Y, He X, Way Y, Lu Y, Gu F, Ball A. Study on failure mechanism of mechanical clinching in aluminum sheet materials. The international journal of advanced manufacturing technology, 2018; 96: 3057 – 3068. https://doi.org/10.1007/s00170-018-1734-2

[3] Lin P-C, Lin J-W, and Li G-X. Clinching process for aluminum alloy and carbon-fiber-reinforced thermoplastic sheets. International Journal of Advanced Manufacturing Technology, 2018; 97: 529-541. https://doi.org/10.1007/s00170-018-1960-7

[4] Lambiase F. Joinability of Different Thermoplastic Polymers with Aluminium AA6082 Sheets by Mechanical Clinching. International Journal of Advanced Manufacturing Technology, 2015; 80:1995–2006. https://doi.org/10.1007/s00170-015-7192-1

[5] Abibe AB, Sônego M, dos Santos JF, Canto LB, Amancio-Filho ST. On the feasibility of friction-based staking joining method for polymer-metal hybrid structures. Materials & Design, 2016; 92: 632 – 642. https://doi.org/10.1016/j.matdes.2015.12.087

[6] Kah P, Suoranta R, Martikainen J, Magnus C. Techniques for joining dissimilar materials: Metals and polymers. Rev. Adv. Mater. Sci., 2014; 36: 152-164

[7] Huang Y, Meng X, Wang Y, Xie Y, Zhou L. Joining of aluminum alloy and polymer via friction stir lap welding. Journal of Materials Processing Tech., 2018; 257: 148-154. https://doi.org/10.1016/j.jmatprotec.2018.02.043

[8] Li Y, Bu H, Yang H, Liu G, Yao J, Zhan X. Effect of laser heat input on the interface morphology during laser joining of CFRTP and 6061 aluminum alloy. Journal of Manufacturing Processes, 2020; 50: 366 – 379. https://doi.org/10.1016/j.jmapro.2019.12.023

[9] Pereira D, Oliveira JP, Santos TG, Miranda RM, Lourenço F, Gumpinger J, Bellarosa R. Aluminium to Carbon Fibre Reinforced Polymer tubes joints produced by magnetic pulse welding. Composite Structures, 2019; 230: 111512. https://doi.org/10.1016/j.compstruct.2019.111512

[10] Mishra R, Ma ZY. Friction stir welding and processing. Mater. Sci. Eng. R., 2005; 50: 1-78. https://doi.org/10.1016/j.mser.2005.07.001
[11] Heinz B, Skrotzki B. Characterization of a friction-stir-welded aluminum alloy 6013. Metallurgical and Materials Transactions B, 2002; 33: 489 - 498. https://doi.org/10.1007/s11663-002-0059-5
[12] Somasekharan AC, Murr LE. Characterization of complex, solid-state flow and mixing in the friction-stir welding (FSW) of aluminum alloy 6061-T6 to magnesium alloy AZ91D using color metallography. Journal of Materials Science, 2006; 41: 5365- 5370. https://doi.org/10.1007/s10853-006-0342-y
[13] Pabandi HK, Movahedi M, Kokabi AH. A new refill friction spot welding process for aluminum/polymer composite hybrid structures. Composite Structures, 2017; 174: 59 – 69. https://doi.org/10.1016/j.compstruct.2017.04.053
[14] Patel AR, Kotadiya DJ, Kapopara JM, Dalwadi CG, Patel NP, Rana HG. Investigation of Mechanical Properties for Hybrid Joint of Aluminium to Polymer using Friction Stir Welding (FSW). Materials Today: Proceedings, 2018; 5: 4242 – 4249. https://doi.org/10.1016/j.matpr.2017.11.688
[15] Liu FC, Dong P, Pei X. A high-speed metal-to-polymer direct joining technique and underlying bonding mechanisms. Journal of Materials Processing Tech., 2020; 280: 116610. https://doi.org/10.1016/j.jmatprotec.2020.116610
[16] Wang H, Yang K, Liu L. The analysis of welding and riveting hybrid bonding joint of aluminum alloy and polyether-ether-ketone composites. J. Manuf. Process, 2018; 36: 301–308. https://doi.org/10.1016/j.jmapro.2018.10.031
[17] Paidar M, Ojo OO, Moghanian A, Pabandi HK, Esla M. Pre-threaded hole friction stir spot welding of AA2219/PP-C30S sheets. Journal of material processing Tech., 2019; 273: 116272. https://doi.org/10.1016/j.jmatprotec.2019.116272
[18] Derazkola HA, Simchi A. An investigation on the dissimilar friction stir welding of T-joints between AA5754 aluminum alloy and poly(methyl methacrylate). Thin-Walled Struct., 2019; 135: 376-384. https://doi.org/10.1016/j.tws.2018.11.027
[19] Lamberti C, Solchenbach T, Plapper P, Possart W. Laser-assisted joining of hybrid polyamide-aluminum structures. Phys. Procedia, 2014; 56: 845–853. https://doi.org/10.1016/j.phpro.2014.08.103
[20] Ojo OO. Macro-/micro-mechanical interlocking modification on the performance of hybrid friction stir spot welded aluminum/acrylonitrile butadiene styrene joints. Research on Engineering Structures & Materials, 2021. https://doi.org/10.17515/resm2021.290me0508
[21] Menghari HG, Babalo V, Fazli A, Soltanpour M, Ziaeipoor H. A study on the electro-hydraulic clinching of aluminum and carbon fiber reinforced plastic sheets. International Journal of Lightweight Materials and Manufacture, 2020; 3: 239 – 249. https://doi.org/10.1016/j.ijlmm.2020.01.002
[22] Liu Y, Zhuang W, Wu S. Damage to carbon fiber reinforced polymers (CFRP) in hole-clinched joints with aluminum alloy and CFRP. Composite Structures, 2020; 234: 111710. https://doi.org/10.1016/j.compstruct.2019.111710
[23] Lambiase F. Mechanical behavior of polymer-metal hybrid joints produced by clinching using different tools. Materials & Design, 2015; 87: 606 – 618. https://doi.org/10.1016/j.matdes.2015.08.037
[24] Lei L, He X, Yu T, Xing B. Failure modes of mechanical clinching in metal sheet materials. Thin-Walled Structures, 2019; 144: 106281. https://doi.org/10.1016/j.tws.2019.106281
[25] Lambiase F, Paoletti A. Friction-assisted clinching of Aluminum and CFRP sheets. Journal of Manufacturing Processes, 2018; 31: 812 – 822. https://doi.org/10.1016/j.jmapro.2018.01.014

[26] Ojo OO. Multi-Objective Optimization of Friction Stir Spot Welds of Aluminum Alloy Using Entropy Measurement. International Journal of Engineering Research in Africa, 2019; 45: 28 – 41. https://doi.org/10.4028/www.scientific.net/jera.45.28
[27] Liang Z-L, Yun T-J, Oh W-B, Lee B-R, Kim I-S. A study on MOORA-based Taguchi method for optimization in automated GMA welding process. Materials Today: Proceedings, 2020; 22: 1778 – 1785. https://doi.org/10.1016/j.matpr.2020.03.011
[28] Ojo OO, Taban E. Hybrid multi-response optimization of friction stir spot welds: failure load, effective bonded size, and flash volume as responses. Sādhanā 2018; 43: 1-13. https://doi.org/10.1007/s12046-018-0882-2
[29] Li C, Huang J, Wang K, Chen Z, Liu Q. Optimization of processing parameters of laser skin welding in vitro combining the response surface methodology with NSGA- II. Infrared Physics & Technology 2019; 103: 103067. https://doi.org/10.1016/j.infrared.2019.103067
[30] Chen FF, Xiang J, Thomas DG, Murphy AB. Model-based parameter optimization for arc welding process simulation. Applied Mathematical Modelling 2020; 81: 386 – 400. https://doi.org/10.1016/j.apm.2019.12.014
[31] Abdollahi A, Shamanian M, Golozar MA. Parametric Optimization of Pulsed Current Gas Arc Welding of Dissimilar Welding Between UNS32750 and AISI 321 Based on Taguchi Method. Trans Indian Inst Met., 2017; 71: 597 – 603. https://doi.org/10.1007/s12666-017-1192-9
[32] Ojo OO, Taban E, Kaluc E. Friction stir spot welding of aluminum alloys: a recent review. Mater. Test., 2015; 57: 609–627. https://doi.org/10.3139/120.110752
[33] Oladimeji OO, Taban E, Kaluc E. Understanding the Role of welding parameters and tool profile on the morphology and properties of expelled flash of spot welds. Materials & Design 2016; 108: 518 – 528. https://doi.org/10.1016/j.matdes.2016.07.013
[34] Mubiayi MP, Akinlabi ET, Makhatha ME. Current trends in friction stir welding (FSW) and friction stir spot welding (FSSW). Structural Integrity, 2019. https://doi.org/10.1007/978-3-319-92750-3
[35] Lambiase F, Paoletti A, Di Hio A. Advances in mechanical clinching: Employment of rotating tool. Procedia Engineering, 2017; 183: 200-205. https://doi.org/10.1016/j.proeng.2017.04.021